NEURAL REGENERATION RESEARCH
Volume 8, Issue 20, July 2013

www.nrronline.org

doi:10.3969/j.issn.1673-5374.2013.20.001 [http://www.nrronline.org; http://www.sjzsyj.org]
Cao JM, Fu D, Li S. A three-dimensional digital visualization model of cervical nerves in a healthy person. Neural Regen Res. 2013;8(20):1829-1836.

A three-dimensional digital visualization model of cervical nerves in a healthy person··

Jiaming Cao[1], Dong Fu[2], Sen Li[3]

1 *Department of Anesthesiology, the 98 Hospital of Chinese PLA, Huzhou 313000, Zhejiang Province, China*
2 *Department of Surgery, Hospital of 8691 People's Armed Police Force, Huzhou 313000, Zhejiang Province, China*
3 *Department of Spinal Surgery, Affiliated Hospital of Luzhou Medical College, Luzhou 646000, Sichuan Province, China*

Research Highlights

(1) We constructed a three-dimensional visualization model of the cervical nerves using Mimics software based on original two-dimensional data obtained by continuous CT angiography and magnetic resonance myelography in a healthy volunteer.
(2) This model represents the first *in vivo* data of cervical nerve anatomy, which differs from classical methods using "visible human" (Digital Human) frozen sections from a cadaver.
(3) This model overcomes the disadvantages of the milling technique and avoids data loss. thermore, vivid images from various angles can be observed due to minimal pattern distortion.

Abstract

Three-dimensional reconstruction nerve models are classically obtained from two-dimensional ages of "visible human" frozen sections. However, because of the flexibility of nerve tissues and small color differences compared with surrounding tissues, the integrity and validity of nerve tissues can be impaired during milling. Thus, in the present study, we obtained two-dimensional data from a healthy volunteer based on continuous CT angiography and magnetic resonance myelography. Semi-automatic segmentation and reconstruction were then conducted at different thresholds in different tissues using Mimics software. Small anatomical structures such as muscles and cervical nerves were reconstructed using the medical computer aided design module. Three-dimensional digital models of the cervical nerves and their surrounding structures were successfully developed, which allowed visualization of the spatial relation of anatomical structures with a strong three-dimensional effect, distinct appearance, clear distribution, and good continuity, precision, and integrality. These results indicate the validity of a three-dimensional digital visualization model of healthy human cervical nerves, which overcomes the disadvantages of milling, avoids data loss, and exhibits a realistic appearance and three-dimensional image.

Key Words

neural regeneration; cervical; three-dimension; CT; magnetic resonance myelography; cervical plexus; phrenic nerve; vagus nerve; recurrent laryngeal nerve; ganglion; stellate ganglion; grants-supported paper; neuroregeneration

Jiaming Cao, Master, Associate chief physician.

Corresponding author: Dong Fu, M.D., Attending physician, Department of Surgery, Hospital of 8691 People's Armed Police Force, Huzhou 313000, Zhejiang Province, China, gdfudong@126.com.

Received: 2012-12-27
Accepted: 2013-03-09
(N20120616002)

Funding: This project was funded by the General Project (class A) of Medical Technology Innovation of Nanjing Military Area in 2011, No. 11MA007.

Author contributions: Cao JM participated in study design, data collection, experiments, and manuscript writing. Fu D and Li S were responsible for data collection. Fu D was in charge of experiment evaluation and manuscript authorization. All authors approved the final version of the paper.

Conflicts of interest: None declared.

Ethical approval: This study was approved by the Ethics Committee, the 98 Hospital of Chinese PLA.

Author statements: The manuscript is original, has not been submitted to or is not under consideration by another publication, has not been previously published in any language or any form, including electronic, and contains no disclosure of confidential information or authorship/patent application/funding source disputations.

INTRODUCTION

The successful implementation of digital "virtual visible human" design has established the foundations for three-dimensional medical visualization techniques[1-2], which include the Visible Human Project dataset established by the National Library of Medicine (USA)[3], the Visible Korean Human dataset[4], and the Virtual Chinese Human dataset[5]. These datasets represent two-dimensional digital images of frozen thin sections. Three-dimensional visual models of many human organs have been established[6-7], which provide valuable digital anatomical images of human organs. Nevertheless, nerve tissues lose their continuity and integrity during the milling performed during sectioning, and it is difficult to distinguish tiny nerve tissues from surrounding tissues owing to the small differences in color. Thus, the two-dimensional images of cervical tissues obtained by milling are distorted and lose some anatomical details.

Studies of three-dimensional visualization of nerve tissues remain in the clinical exploratory stage[8], and the optimal types of original materials for three-dimensional reconstruction remain unclear. In particular, there are no reports addressing successful three-dimensional construction of visualization models of nerve tissue *in vivo*. Previous studies have confirmed that continuous CT angiography and magnetic resonance myelography can reveal continuous, complete, and precise two-dimensional original data[9-10]. These advances in image processing have provided the basis for three-dimensional visualization models of living tissues[9-10].

The established anatomical structure of cervical nerves is based on morphological observation and studies of nerve block anesthesia and treatment, including cervical plexus block, stellate block, paravertebral nerve block, superior laryngeal nerve block, and recurrent laryngeal nerve block. However, cervical tissues are complicated, and nerve block or operation on the neck can induce complications in the surrounding tissues. For example, straying into the subarachnoid cavity would cause total spinal anesthesia, resulting in respiratory and cardiac arrest[11-12]. Phrenic nerve block can also damage respiratory function[13-14], while straying into the sheath of cervical vessels leads to a toxic reaction of local anesthetics[15]. Furthermore, an anterior approach in the cervical vertebra may damage the sympathetic ganglion and vagus nerve[16].

There are few data concerning three- dimensional visualization applied anatomy of the cervical nerves *in vivo*. As such, we collected continuous, complete, and precise two-dimensional original data based on continuous CT angiography and magnetic resonance myelography. A three-dimensional visualization model of the cervical nerves was then established using Mimics software. As this model was obtained from a living body rather than a cadaver, it overcomes the disadvantages of milling, avoids data loss, and exhibits a realistic three-dimensional appearance. The original data for this model are easy to obtain, which greatly decreases the costs and allows further investigations. This model revealed the morphology, distribution, and spatial relations of the major nerves of the neck, and provided three-dimensional morphological data for anatomical teaching and morphological observation of regenerated nerves, nerve block anesthesia, and surgery.

RESULTS

Identification of three-dimensional visualization models of the cervical nerves and surrounding structures

A healthy volunteer received continuous CT angiography and magnetic resonance myelography. A three-dimensional model of the cervical nerves and surrounding structures was constructed using Mimics software based on the geometrical features of the models' surface. The model included the skeletal system, arterial and venous systems (ascending aorta, aortic arch, subclavian artery, common carotid artery, verte

bral artery, external jugular vein, internal jugular vein, subclavian vein, superior thyroid artery, and inferior thyroid artery), nervous system (spinal cord, spinal ganglia, ramus communicans of spinal nerve, cervical plexus cutaneous branch, phrenic nerve, root, trunk, bundle and brachial plexus, cervical segment of the vagus nerve, cervical sympathetic nerve trunk, cervical sympathetic ganglia, superior laryngeal nerve, and recurrent laryngeal nerve), and muscle tissue (sternocleidomastoid, scalenus medius, and lavatory scapulae muscle).

The three-dimensional reconstruction model is shown in Figures 1–4. The spatial relations of the different cervical nerves and surrounding anatomical structures are shown in Figures 1–3. The three-dimensional visualization model of the cervical nerves and surrounding structures is shown in Figure 4.

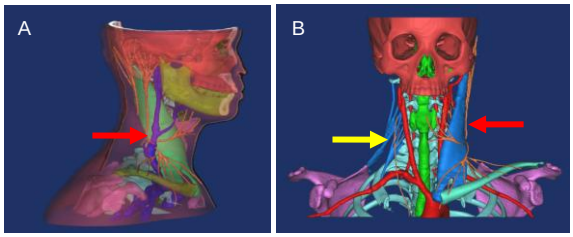

Figure 1 Morphology of the cervical plexus cutaneous branch (lesser occipital nerve, great auricular nerve, transverse nerve of the neck, and supraclavicular nerves) and phrenic nerve in a three-dimensional digital visualization model of the cervical nerves.

(A) Percutaneous perspective section. Red arrow shows the correlation between the cervical plexus cutaneous branch (four branches) and the sternocleidomastoid and external jugular vein. The skin is transparent.

(B) Anterior view of the cervical plexus branch. Red arrow shows the cervical plexus cutaneous branch (transverse nerve of the neck and supraclavicular nerves). Yellow arrow shows the phrenic nerve.

Figure 1 mainly shows the cervical plexus cutaneous branch and phrenic nerve. The cervical plexus is located in the deep part of the sternocleidomastoid, with the presence of branches, cutaneous branches (lesser occipital nerve, great auricular nerve, transverse nerve of neck, and supraclavicular nerves), and phrenic nerve. Figure 1A shows the percutaneous perspective section, in which the skin is totally transparent. This section shows the relation between the cervical plexus cutaneous branches (four) and the sternocleidomastoid, external jugular vein; from right to front: lesser occipital nerve, great auricular nerve, transverse nerve of the neck, and supraclavicular nerves (semitransparent skin). The cervical plexus cutaneous branch is distributed around from the midpoint of the posterior border of the sternocleidomastoid by traversing the superficial layer of the deep fascia of the neck under the skin. The lesser occipital nerve ascends along the posterior border of the sternocleidomastoid in the skin of the occipitalia. The great auricular nerve is located in front of the superficial part of the sternocleidomastoid, and is distributed in the auricle and its surrounding skin. Figure 1B shows the anterior view of the cervical plexus branch. The left half of the figure indicates the morphology and distribution of the transverse nerve of the neck and the supraclavicular nerves. The transverse nerve of the neck fans transversely out from the superficial part of the central sternocleidomastoid forward, and is distributed in the skin of the anterior portion of the neck. The supraclavicular nerves give off several branches and are distributed in the skin of the lateral-to-anterior aspect of the neck, above the second rib of the anterior chest wall and shoulder. The right half of the figure shows the levator scapulae muscle, scalenus medius, and the right phrenic nerve. The phrenic nerve is composed of the third, fourth, and fifth pairs of the anterior branch of the cervical nerves, and runs posterior to the subclavian vein and anterior to the internal thoracic artery as it enters the thorax.

Figure 2 shows the relation between the cervical segments of the vagus nerve, superior laryngeal nerve, and the recurrent laryngeal nerve to the aorta. The vagus nerve descends in the neck, posterior to the common carotid artery, and enters the thorax through the superior aperture of the thorax. The left recurrent laryngeal nerve originates at the aortic arch, branches from the vagus nerve to loop under the arch of the aorta, posterior to the ligamentum arteriosum, before ascending and entering into the pharynx posterior to the cricothyroid joint. By contrast, the right branch loops around the right subclavian artery, and enters the pharynx posterior to the cricothyroid joint.

Figure 2C shows the relation between the cervical segments of the vagus nerve, superior laryngeal nerve, recurrent laryngeal nerve, and cervical sympathetic trunk (cervical segments of vagus nerve are semitransparent). The cervical sympathetic trunk is distributed exterior to the cervical spinal column, posterior to the sheath of the cervical vessels (one on the left, one on the right). The cervical sympathetic trunk contains the superior cervical ganglion, middle cervical ganglion, and the inferior cervical ganglion, from top to bottom. The cervicothoracic ganglion is formed by fusion of the inferior cervical ganglion and the first thoracic ganglion.

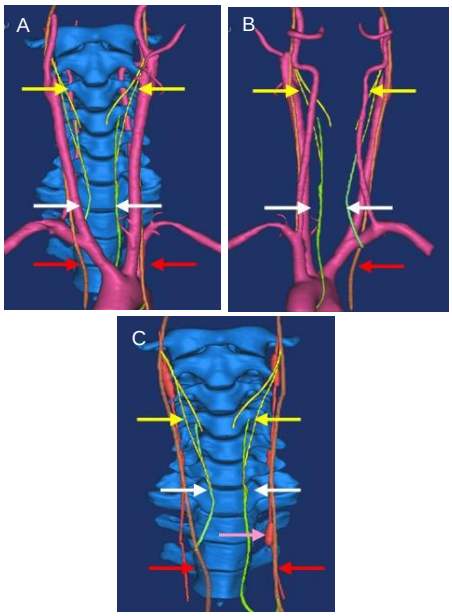

Figure 2 Morphology of the cervical segments of the vagus nerve, superior laryngeal nerve, and the recurrent laryngeal nerve, and their correlation to the aorta in a three-dimensional digital visualization model of the cervical nerves.

(A) Anterior view. (B) Posterior view. (C) Semitransparent view. Red arrows: the relation between cervical segments of the vagus nerve and the carotid artery. Yellow arrows show the relation between the superior laryngeal nerve and the carotid artery. White arrows show the relation between the recurrent laryngeal nerve and the carotid artery. Pink arrow shows the relation between the cervical sympathetic trunk and the carotid artery.

Figure 3 shows the relation between the superior laryngeal nerve and the recurrent laryngeal nerve to the superior and inferior thyroid arteries (semitransparent aorta). The superior laryngeal nerve branches from the main trunk of the vagus high in the neck, and then descends in the neck adjacent to the pharynx. It is separated into the internal branch and the external branch. The internal branch of the superior laryngeal nerve accompanying the superior laryngeal artery and superior laryngeal vein enters the larynx through the thyrohyoid membrane. The very small external branch reaches the superior pole of the thyroid gland by coursing with the blood vessels of the thyroid gland, which innervates the cricothyroid muscle. As shown in Figure 3, on the superior pole of the thyroid gland, the superior laryngeal nerve enters the larynx anterior to and below the inferior horn of the thyroid cartilage. On the inferior pole of the thyroid gland, the recurrent laryngeal nerve crosses the branches of the inferior thyroid artery. The region between the poles is termed the ‘dangerous area’, as it is easy to damage these two segments of the nerves during surgery.

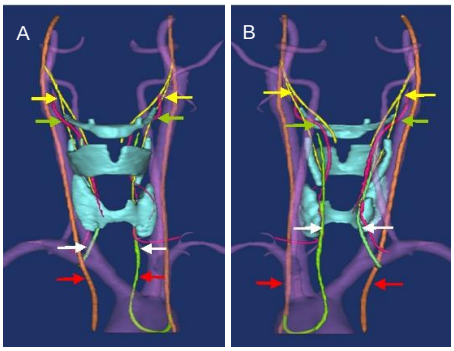

Figure 3 Three-dimensional graphics of the superior laryngeal nerve, recurrent laryngeal nerve, and the thyroid artery in a three-dimensional digital visualization model of the cervical nerves.

This picture demonstrates the relation of the superior laryngeal nerve (yellow arrows) and the recurrent laryngeal nerve (white arrows) to the superior thyroid artery and the inferior thyroid artery (green arrows) (aorta is semitransparent). Red arrows show a semitransparent cervical branch of the vagus nerve. (A) Anterior view. (B) Posterior view.

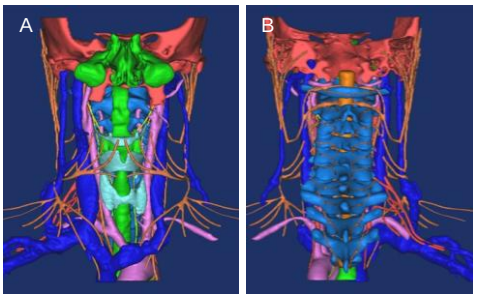

Figure 4 The three-dimensional digital visualization model of the cervical nerves. The internal structure of each component can be observed from different angles or cross-sections.

(A) Three-dimensional digital visualization model of the cervical plexus, vagus nerve, superior laryngeal nerve, recurrent laryngeal nerve, thyroid gland, carotid artery, jugular vein, superior thyroid artery, and the inferior thyroid artery (anterior view).

(B) Three-dimensional visualization model of the cervical nerves (posterior view).

Characteristics of the three-dimensional digital visualization model of the cervical nerves

We used the three-dimensional digital visualization model of the cervical nerves established in this study to observe their internal structure from different angles or cross-sections. This model can be reduced or magnified, and permeabilized (Figures 1A, 2C), pseudo-colored (Figures 1–4), or materialized. The cervical nerves displayed using this model presented a strong stereoscopic and vivid appearance, with a clear distribution and good

continuity, precision, and integrity.

DISCUSSION

Advantages of the reconstructed three-dimensional visualization models

"Medical image visualization" is a novel medical research field. Medical two-dimensional images are commonly obtained by cadaver frozen sections, CT, MRI, and ultrasound[17-18]. Two-dimensional data of well-known "digital visualization human" samples are obtained using frozen thin sections[19]. Many countries including the USA and China have digital visualization human datasets[20-22], and there are numerous studies that have digitally reconstructed multiple human organs or body parts. However, because of the flexibility of nerve tissues and the small color differences between the tiny nerves and surrounding tissue, the integrity and validity of nerve tissues is reduced due to tearing during milling. The collection of frozen sections also depends on good management, storage, perfusion, and cutting of the cadaver, and the data collection and later processing requires tremendous manpower and material resources[23]. With the advances in computerized processing image techniques, there has been rapid development and application of visualization techniques[24-25].

We previously reported our original two-dimensional data based on spiral CT angiography and magnetic resonance myelography[26], from which we constructed a three-dimensional digital visualization model of the cervical nerves. This model showed a strong three-dimensional effect, distinct appearance, clear distribution, and good continuity, precision, and integrity. We also solved the topological problem of isosurfaces generated by the Marching Cubes method. Thus, the use of intact two-dimensional images and good three-dimensional reconstruction methods effectively overcomes the shortcomings of the milling technique and avoids data loss. Three-dimensional visualization model data are also easier to compare than a cadaver, which decreases costs and improves the feasibility of the study of nerves or morphology of neural regeneration *in vivo*.

Significance of three-dimensional visualization of the cervical nerves

Medical teaching of the relation between the cervical nerves and surrounding tissues mainly uses gross anatomical specimens and atlases. However, the anatomical specimens typically exhibit some degree of tissue damage due to the handling and storage of the cadaver, which alters the spatial structure. Thus, students cannot gain a complete understanding of the anatomical structures. Furthermore, when using the two-dimensional anatomical atlases, the students have to imagine the three-dimensional relations.

Using Mimics software, two-dimensional images can be identified and separated with a PC, and three-dimensional reconstruction can be performed. In the present study, our digital visualization model could display complicated tissues using various colors and multiple structures. This model could clearly show the cervical plexus cutaneous branch, phrenic nerve, vagus nerve, superior laryngeal nerve or recurrent laryngeal nerve, cervical sympathetic nerve trunk, cadre, blood vessels, and muscle. In the three-dimensional position, all structures can be rotated along any axis and angle, and can be magnified. Reconstructed images can also be animated for dissection, rotation, and recombination in any direction, which is useful for medical teaching and clinical treatment[27]. Therefore, the digital visualization model can be used as a supplement for teaching material and anatomical atlases[27].

Previous studies examining nerve injury and the morphology of regeneration have used three-dimensional reconstruction of tissue sections[28-29], while there are no reports that utilize *in vivo* tissues. In the present study, we performed three-dimensional reconstruction using the imaging technique *in vivo*, which provides a useful data for future studies on nerve tissue injury or morphology of regeneration.

Our three-dimensional image data of the cervical nerves can also be utilized to examine nerve blocking anesthesia puncture or surgical simulation. Cervical nerve block at the cervical plexus, brachial plexus, or cervical sympathetic nerve is a commonly used anesthetic or therapeutic method for neck operations. However, owing to the position of the cervical nerve, if the position of the nerve block is not precise, total spinal anesthesia can occur, which may cause cardiac arrest, local anesthetic intoxication, and pneumothorax. Thus, it is important to determine the exact anatomical position and spatial structure of the neck to improve therapeutic outcomes and to reduce complications.

In this study, the three-dimensional reconstruction models could be used to view the local or entire cervical nerves and surrounding structures. Different tissues were displayed by different colors and transparencies, and we could clearly observe the relative positions and relations of

the cervical nerves and the spinal cord, bone structure, cervical vessels, sternocleidomastoid, scalenus medius, and levator scapulae muscle. Thus, this model allows us to accurately measure the three-dimensional organization of the cervical nerves, which would be useful for anesthetic or surgical operators to accurately determine the position, depth, direction and angle of puncture pin for puncture procedures, and incision site and size for surgery. This model also allows precise location of nerves, which allows surgeons to select the optimal surgical path and reduce complications.

In summary, we successfully constructed a three-dimensional digital visualization model of the cervical nerves. This model can provide anatomical morphology reference data for nerve blocking anesthesia, morphological observation, and clinical surgery. Nevertheless, as we used only one subject, future studies with a larger number of subjects are required.

SUBJECT AND METHODS

Design

A computer simulation, neuroimaging study.

Time and setting

Experiments were performed at the Department of Radiology, the 98 Hospital of Chinese PLA, China from May 2011 to November 2011.

Subject

A female healthy volunteer aged 25 years (weight, 52 kg; height, 163 cm) was selected from the 98 Hospital of Chinese PLA. The subject had no history of rheumatism or heart disease. Cervical X-ray film was normal (Figure 5). Injury, deformation, and other lesions were excluded. The subject was informed of the protocols and risks before experiments in accordance with *Administrative Regulations on Medical Institution*, formulated by State Council of the China[30]. The subject signed informed consents.

Methods

Computer

Dell graphic workstation (Dell, Austin, TX, USA), version: Precision M90; processor: Intel Core 2 Duo T7200; memory: 2G DDR2-667 SDRAM; hard disc: 160 GB; video card: NVIDIA Quadro FX 1500M; 256 M video memory; 24 inches of liquid crystal display.

Computer operating system

Windows XP Professional SP2. 3D medical picture editing handling software Mimics 14.11 (Materialise, Leuven, Belgium) was used to handle fault data and three-dimensional model construction.

Figure 5 X-ray examination of the cervical part at the anterior view of a female healthy volunteer aged 25 years.

No abnormal lesion was found in this subject. L: Left.

Collection of original data

Continuous CT non-contrast enhanced scan and CT angiography were conducted using an Aquilion 64 spiral CT (Toshiba, Tokyo, Japan). The scan plane was from the head to the inferior border of the third thoracic vertebra, along the cross section. Scanning condition: collimating device width 49.970 mm × 0.976 mm, tube tension 120 kV; soft tissue window was selected.

CT angiography: Ultravist (iopromide injection, 370 mg/mL; Xianling Pharmacy Co., Ltd., Guangzhou, Guangdong Province, China) 80 mL, at a flow rate of 5 mL/s, was intravenously injected *via* the left antecubital vein. Subsequently, 30 mL of saline was injected at a flow rate of 3 mL/s. Following CT non-contrast enhanced scan, continuous scanning was performed at the arterial phase and the venous phase. The plain scan phase, arterial phase, and venous phase each contained 670 slices. Original data reconstruction: slice thicknes 0.5 mm, spacing 0.5 mm, matrix 512 × 512.

A Trio Tim 3.0 T superconducting magnetic resonance scanner (Siemens, Berlin, Germany) was used for magnetic resonance myelography. Cross section scanning was conducted from the head to the inferior border of the third thoracic vertebra. Scanning parameters: 2 mm slice thickness, 4.92 ms inversion time, 14 ms echo time, 500 mm display field of view, and 512 × 512 matrix, no repeats. Data storage mode was Dicom 3.0 standard[31].

Reconstruction of the three-dimensional digital visualization model of the cervical nerves

Dicom format fault images were introduced into Mimics

software (Materialise). The contrast, window level, and window width were adjusted. Images were positionally matched to subvoxel accuracy using the interpolation technique.

The interest point in one image in each slice was selected. Closed contour segmentations of the scanned images were performed using Mimics software. The three-dimensional model was viewed using different intensities of light.

Based on different CT thresholds of skeleton, skin, and trachea, contour line extraction at different thresholds was performed using the thresholding tool (Materialise). The Contour Line Extraction Algorithm Based on Region Growing is presented. Three-dimensional digital models of the cervical vertebra, first-third thoracic vertebra, maxilla and mandible, clavicle, sternum and scapula, skin, and trachea were constructed using semi-automatic segmentation.

Based on the different CT thresholds of the artery, vein, thyroid gland, and laryngeal cartilage at different phases of angiography, the contour line extraction was performed using thresholding. A dynamic region growing technique, which enhanced image segmentation results, was used for construction of the three-dimensional digital model of the ascending aorta, aortic arch, subclavian artery, common carotid artery, vertebral artery, superior thyroid artery, inferior thyroid artery, external jugular vein, internal jugular vein, subclavian vein, thyroid gland, hyoid bone, laryngeal cartilage (thyroid cartilage), and the sternocleidomastoid. Redundant data were removed. The C_1–T_3 spinal cord was segmented using region growing. A three-dimensional digital model of the C_1–T_3 spinal cord was constructed using the Marching Cubes algorithm[32]. Medical computer-aided design was used for manipulating the relation between the nerves and the surrounding structures. Nerve pipe editor was utilized to identify the position of the key point of different nerves, which was connected with a line of different diameters to simulate nerve morphology, distribution, and size. Subsequently, a digital model of the spinal ganglia, communicating branch, brachial plexus root, trunk, bundle, cervical segments of vagus nerve, cervical sympathetic nerve trunk, cervical sympathetic ganglia (superior cervical ganglion, middle cervical ganglion, cervicothoracic ganglion), cervical plexus cutaneous branch (supraclavicular nerves, transverse nerve of the neck, great auricular nerve, lesser occipital nerve), phrenic nerve, superior laryngeal nerve (internal and external branches), recurrent laryngeal nerve, levator scapulae muscle, and scalenus medius was created. Different anatomic structures were distinguished by pseudo coloring. The three-dimensional model was revealed by a triangular patch. The model was then exported using STL format.

Validation of the three-dimensional digital visualization model of the cervical nerves

Clinical medical experts and imaging experts compared the three-dimensional model results to the human anatomical structure to verify the accuracy and rationality of this model. The modeling standard was in accordance with the morphological characteristics and the geometrical modeling technique. Tissue structure checking contained geometric topology, size, shape, branch, hole, and density of various tissue structures[20].

After three-dimensional model construction, different tissues were shown by different pseudo colors. Very small structures could be magnified or hyalinized. The spatial relation between different structures could be observed by using different angles or cross sections.

REFERENCES

[1] Yuan L, Huang WH, Tang L. The general research situation of visible virtual human. Zhongguo Linchuang Jiepouxue Zazhi. 2002;20(5):341-344.

[2] Schubert R, Schiemann T, Tiede U, et al. Applications and perspectives in anatomical 3-dimensional modelling of the visible human with VOXEL-MAN. Acta Anat (Basel). 1997;160(2):123-131.

[3] Slavin KV. The Visible Human Project. Surg Neurol. 1997;48(6):638-639.

[4] Park JS, Chung MS, Hwang SB, et al. Visible Korean human: improved serially sectioned images of the entire body. IEEE Trans Med Imaging. 2005;24(3):352-360.

[5] Zhong SZ, Yuan L, Tang L, et al. Research report of experimental database establishment of digitized virtual Chinese No.1 female. Diyi Junyi Daxue Xuebao. 2003;23(3):196-200.

[6] Dai JX, Chung MS, Qu RM, et al. The Visible Human Projects in Korea and China with improved images and diverse applications. Surg Radiol Anat. 2012;34(6):527-534.

[7] Chen G, Li XC, Wu GQ, et al. Three-dimensional reconstruction of digitized human liver: based on Chinese Visible Human. Chin Med J (Engl). 2010;123(2):146-150.

[8] Chen J, Peng CL, Chu YF, et al. Visualization of regenerated sciatic nerve of rat after injury. Shengwu Yixue Gongchengxue Zazhi. 2005;22(2):324-326.

[9] Xu TF, Duan WC, Lu T, et al. Application of three-dimensional reconstruction technique based on CT-MRI fusion in skull base surgery. Zhonghua Er Bi Yan Hou Tou Jing Wai Ke Za Zhi. 2012;47(5):373-378.

[10] Pin HY, Long TH, Chen WX. Spiral CT scanning and multimode three-dimensional reconstruction in diagnosis and treatment of lumbar intervertebral disc herniation. Zhongguo Zuzhi Gongcheng Yanjiu yu Linchuang Kangfu. 2011;15(22):4146-4149.
[11] Li N, Liang M, Zhou DH. A case report of whole spinal anesthesia under neurostimulator guides. Linchuang Mazuixue Zazhi. 2007;23(5):411.
[12] Chen XR, Peng DZ, Ye JM. A case report of whole spinal anesthesia from interscalene brachial plexus block. Gannan Yixueyuan Xuebao. 2006;26(2):268.
[13] Liu Y, Jin BL. Clinical study of suitable ropivacaine concentration in brachial plexus block. Zhongguo Linchuang Yanjiu. 2011;(5):405-406.
[14] Mulroy MF. Advances in regional anesthesia for outpatients. Curr Opin Anaesthesiol. 2002;15(6):641-645.
[15] Saeki S, Kobayashi M, Miyake E, et al. Crisis management during regional anesthesia including peripheral nerve block, epidural anesthesia and spinal anesthesia. Masui. 2009;58(5):595-603.
[16] Sansur CA, Reames DL, Smith JS, et al. Morbidity and mortality in the surgical treatment of 10,242 adults with spondylolisthesis. J Neurosurg Spine. 2010;13(5):589-593.
[17] Kovacs A, Mohlenbruch M, Hadizadeh DR, et al. Noninvasive imaging after stent-assisted coiling of intracranial aneurysms: comparison of 3-T magnetic resonance imaging and 64-row multidetector computed tomography--a pilot study. J Comput Assist Tomogr. 2011;35(5):573-582.
[18] McMahon EM, Jiamsripong P, Katayama M, et al. Accurate guidance of a catheter by ultrasound imaging and identification of a catheter tip by pulsed-wave Doppler. Pacing Clin Electrophysiol. 2012;35(1):44-50.
[19] Zhang YZ, Yin B, Huang WH. Visualization of anatomic structures of the normal brachial plexus of the VCH Female I. Zhonghua Shouwaike Zazhi. 2005;21(5):24-26.
[20] Ackerman MJ. The Visible Human Project: a resource for anatomical visualization. Stud Health Technol Inform. 1998;52 Pt 2:1030-1032.
[21] Zhong SZ. Actualities and prospects of research on digitized virtual human. Jiefangjun Yixue Zazhi. 2003;28(5):385-388.
[22] Zhang SX, Heng PA, Liu ZJ. Chinese visible human project. Clin Anat. 2006;19(3):204-215.
[23] Park JS, Chung MS, Hwang SB, et al. Visible Korean Human: its techniques and applications. Clin Anat. 2006;19(3):216-224.
[24] Tang M, Chen F, Tao L. Research progress and development direction of visualization and accelerating techniques for medical images. Zhongguo Zuzhi Gongcheng Yanjiu yu Linchuang Kangfu. 2011;15(4):741-744.
[25] Yu JL, Huang ZH, Fu D. Reconstruction of a digital three-dimensional model of the rectum and the surrounding structures based on CT angiographic data. Nanfang Yike Daxue Xuebao. 2008;28(8):1466-1468.
[26] Fu D, Jin AM, Cao JM, et al. Three-dimensional construction and visualization of cervical plexus and its surrounding structures. Jiefangjun Yixue Zazhi. 2010;35(5):555-557.
[27] Zhang SX, Liu ZJ, Qiu MG, et al. Visualization of the first Chinese visible human male and female. Disan Junyi Daxue Xuebao. 2003;25(7):563-565.
[28] Chen J, Chu YF, Zhu G, et al. Three-D reconstruction for morphology of regenerating sciatic nerve in rats. Disan Junyi Daxue Xuebao. 2002;24(5):591-593.
[29] Wu C, Yang L, Dai P, et al. Relation between 3-d reconstruction of regenerated fibers and functional recovery after mastoid segment of facial nerve was repaired. Lin Chang Er Bi Yan Hou Tou Jing Wai Ke ZaZhi. 2011;25(19):895-898.
[30] State Council of the People's Republic of China. Administrative Regulations on Medical Institution. 1994-09-01.
[31] Fan SF, Yi Z, Xu Z, et al. Clinic application of Epub of medical imaging film in CT workflow. Eur J Radiol. 2011;80(3):e552-556.
[32] Enderling H, Anderson AR, Chaplain MA, et al. Visualisation of the numerical solution of partial differential equation systems in three space dimensions and its importance for mathematical models in biology. Math Biosci Eng. 2006;3(4):571-582.

(Reviewed by Dean J, Stow A, Zhang JM, Liu B)
(Edited by Wang J, Qiu Y, Li CH, Song LP, Liu WJ, Zhao M)